Applied Catalysis B: Environmental 303 (2022) 120921

Contents lists available at ScienceDirect

Applied Catalysis B: Environmental

journal homepage: www.elsevier.com/locate/apcatb

Thermodynamically controlled photo-electrochemical CO_2 reduction at Cu/rGO/PVP/Nafion multi-layered dark cathode for selective production of formaldehyde and acetaldehyde

Amol U. Pawar [a], Umapada Pal [a,b], Jin You Zheng [a,c], Chang Woo Kim [d], Young Soo Kang [a,*]

[a] Department of Chemistry, Sogang University, #1 Shinsu-dong, Mapo-gu, Seoul 121-742, Republic of Korea
[b] Institute of Physics, Autonomous University of Puebla, Mexico
[c] Engineering Research Center of Advanced Functional Material Manufacturing of Ministry of Education, School of Chemical Engineering, Zhengzhou University, Zhengzhou 450001, China
[d] Department of Nanotechnology Engineering, College of Engineering, Pukyong National University, Busan 48513, Republic of Korea

ARTICLE INFO

Keywords:
Photo-electrochemical CO_2 reduction
Product selectivity
CO_2 capture & activation
Reduction potential tunning
In situ Raman/ATR-IR

ABSTRACT

Transforming greenhouse gases such as CO_2 to energy rich carbon-based chemicals is considered as one of the most efficient technologies for environmental and energy sustainability. However, CO_2 is highly stable molecule and difficult to reduce due to its linear structure. The rate of reduction and the nature of fuel product depend on the kinetics and thermodynamics of involved reactions. While the overall reaction kinetics depends on the energy of activated CO_2 molecule and its subsequent transition states along with reduction dynamics. Here we demonstrate that by activation of thermodynamically stable CO_2 molecule through complexation or coordination with suitable activator such as N-heterocyclic polymers (e.g., poly(4-vinyl)pyridine, PVP), both the kinetics and thermodynamics of photoelectrochemical CO_2 reduction reaction can be controlled by proper choice of electrode materials and bias potential. We present a solar light driven photoelectrochemical process for producing formaldehyde and acetaldehyde selectively on multi-layered Cu/rGO/PVP/Nafion hybrid cathode.

1. Introduction

Substantial increase of atmospheric CO_2 concentration is considered as the principal reason for current global warming and subsequent climate change [1–5]. While a collective global effort for the reduction of CO_2 emission is in place, conversion of ambiental CO_2 into useful hydrocarbon fuel is beneficial not only to keep in check the global warming, but also as useful contribution towards current energy demand. Several methods such as thermo-catalytic hydrogenation under high temperature and pressure [6], photocatalytic (PC) reduction [7–10], photothermal reduction [11,12], electrochemical (EC) reduction [13–17], biological and photoelectrochemical (PEC) reduction [18–20] have been utilized recently for the conversion of CO_2 into useful hydrocarbons. However, these methods further modified by using MOF assisted catalysis materials [21–23]. Among them, thermo-catalytic hydrogenation and electrochemical processes, although deemed efficient, suffer from high input energy cost and lack of product selectivity. On the other hand, in natural biological processes such as in plants, while the CO_2 reduction occurs under optimum reaction conditions to produce glucose, the reaction is not kinetically controlled (solar energy conversion efficiencies of most of the plants is less than 1%) [24,25]. The slow kinetics of CO_2 reduction in the natural photosynthesis process even with perfect thermodynamic control over product selectivity is associated to the reaction of plant (also of microbes such as bacteria) enzymes with CO_2 molecules at lower collision frequencies [25]. Therefore, it is necessary to study the reaction kinetics of CO_2 reduction in optimum thermodynamic conditions to enhance the solar to fuel (STF) conversion efficiency in artificial photosynthesis processes.

Several research groups have reported the EC reduction of CO_2, both theoretically and experimentally, proposing possible reaction pathways [26–32]. However, the main problems associated with EC reduction of CO_2 are the high overpotential and lack of product selectivity. The high overpotential required for CO_2 reduction is the reason behind the lower Faradaic efficiency (FE) or current efficiency of electrochemical CO_2 reduction processes [26–28]. Lack of product selectivity and low Faradaic efficiency of electrochemical CO_2 reduction are the result of

* Corresponding author.
E-mail address: yskang@sognag.ac.kr (Y.S. Kang).

https://doi.org/10.1016/j.apcatb.2021.120921
Received 9 September 2021; Received in revised form 2 November 2021; Accepted 9 November 2021
Available online 16 November 2021

simultaneous occurrence of two inter-competing reactions, i.e. generation of hydrogen and reduction of CO_2 in the cathode compartment [33,34]. On the other hand, solar photocatalytic CO_2 reduction is a simpler process. However, as the only energy source involved in solar photocatalytic reduction process is the external one (solar radiation), product selective reduction of CO_2 is almost impossible. Moreover, the efficiency of solar CO_2 reduction producing liquid fuel in solar photochemical process is limited by water splitting. In contrast, in PEC process, as the reduction potential can be controlled through external bias, we can overcome such limitation to enhance CO_2 reduction efficiency. Therefore, PEC is considered to be one of the most convenient processes for product-selective reduction of CO_2. The generation of CO [35], methane [36], methanol [37], formic acid and formaldehyde [19,38] have been demonstrated through PEC reduction of CO_2.

Recently, Aguirre et al. reported multi-layered photo-electrochemical CO_2 reduction towards methanol with FTO/Cu/Bi_2Se_3-Se/Cu_2O as a photocathode [39]. However, in most of the cases these photocathodes suffer from long term stability during photocatalytic reaction. Utilizing such multi-layered electrodes as dark cathode seems to be the best option to overcome this problem. Recently Kang et al. reported the utilization of rGO-based dark cathodes showing their good performance in CO_2 reduction reaction for producing alcohol selectivity [20,37]. Yet, lack of product selectivity and low conversion efficiency are the two aspects which require further attention. To attend these problems, it is necessary to develop innovative cathode materials or multi-component cathodes containing layers of specific functionalities, which not only can improve the product selectivity of the process, but also can enhance the CO_2 reduction rate by lowering the activation energy, especially for the first electron transfer (which is the rate determining step) from cathode to CO_2 molecules adsorbed at their surfaces.

In this study, we demonstrate a novel strategy for selective and controlled production of formaldehyde and acetaldehyde through PEC reduction of CO_2. Utilizing calcium (Ca) and iron (Fe) co-doped TiO_2 (TiO_2:Ca-Fe) films as photoanode and Cu/rGO/PVP/Nafion multi-layered electrode as cathode, formaldehyde and acetaldehyde could be generated selectively at cathode surface by tuning anode bias potential. Product selectivity in the CO_2 reduction process was monitored in situ utilizing gas chromatography (GC). The first electron transfer process, i.e., the formation of $CO_2^{-\bullet}$ radical at cathode surface was monitored through in situ electron paramagnetic resonance (EPR). Formation of CO_2 reduction intermediates during the process was monitored by in situ ATR-IR and Raman spectroscopies. The 4-electron transfer involved in CO_2 reduction process was probed by time-resolved chronoamperometry using Au ultra-microelectrode. Considering all the thermodynamic aspects, possible reaction pathways for formaldehyde and acetaldehyde generation have been outlined.

2. Experimental methods

2.1. Materials

Calcium acetate monohydrate ($Ca(CH_3COO)_2{\cdot}H_2O$, 99.99%), iron (III) nitrate nonahydrate ($Fe(NO_3)_3{\cdot}9H_2O$, ≥98.0%), polyethylene glycol ($C_{2n}H_{4n+2}O_{n+1}$, PEG 8000), titanium foil (2.0 mm thick, 99.7%), sodium hydroxide (NaOH), graphite flakes (+100 mesh), poly(4-vinylpyridine) average Mw ~160,000 (PVP), copper foil thickness 0.5 mm (99.98% trace metals basis), and copper sulfate ($CuSO_4$, ≥ 99%) were acquired from Sigma-Aldrich, Korea, and utilized as received, without further purification. Deionized (DI) water from a Milli-Q gradient (Quantum EX cartridge filter included) Millipore system was used throughout for washing and electrolyte preparation. A perfluorinated Nafion resin solution (Nafion D2021, Fuel Cell Store, USA) containing 46 wt% of aliphatic alcohols and 34 wt% of water was used for electrode preparation.

2.2. Synthesis

2.2.1. Synthesis of $CaFe_2O_4$ (CFO) nanoparticles

For the fabrication of CFO nanoparticles, first a solution was prepared by dissolving 2.0 mmol calcium acetate and 4.0 mmol iron (III) nitrate in 20 mL of DI water. A 5.0 mL aqueous solution of polyethylene glycol (5.0 wt%) was then added to the previous solution. The mixture solution was then heated at 120 °C for 2 h under vigorous magnetic stirring. The reaction mixture was then cooled down to room temperature. Produced nanoparticles were then separated by centrifugation, washed several times with DI water, and air-dried at room temperature overnight. Obtained powder sample was then air-annealed successively, first at 450 °C for 2 h and then at 1050 °C for 4 h.

2.2.2. Fabrication of Ca-Fe doped TiO_2 (TiO_2:Ca-Fe) photoanode

For the fabrication of TiO_2:Ca-Fe photoanodes, first we fabricated the CFO films over commercial Ti foils utilizing doctor-blade method. A dense CFO paste was prepared by mixing 1.0 g of annealed CFO powder and 0.5 g of polyethylene glycol (PEG 8000) in 1.5 mL of DI water under magnetic stirring. The paste was then ultrasonicated for 10 min and utilized for film deposition over Ti foils. Fabricated CFO films were annealed at different temperatures (900, 1000 and 1100 °C) in Ar atmosphere (50 sccm flow rate). The high temperature (≥ 900 °C) annealing induced a reaction between the surface of the Ti foil and CFO particles over it, producing a thin TiO_2 layer over the Ti foil. A prolonged annealing at high temperature causes the diffusion of Ca and Fe atoms into the formed TiO_2 layer, producing Ca and Fe co-doped TiO_2 (TiO_2:Ca-Fe) film at the surface of the Ti foil. The TiO_2:Ca-Fe film prepared in this way was utilized as photoanode for PEC reduction of CO_2. The whole process of photoanode fabrication has been depicted schematically in Fig. S16 (Supporting Information).

2.2.3. Fabrication of multi-layered hybrid composite cathode

Four different types of cathodes were fabricated for a comparative CO_2 reduction study. The Cu/rGO cathodes were prepared by dip-coating. For that, polished Cu foils of 2 × 2 cm^2 sizes were simply immersed into GO solution (1 mg/mL in water) for 10 h. The prolonged immersion of Cu foil into the GO solution not only induced the reduction of GO to rGO, the formed rGO flakes also assembled over the Cu foil as has been reported by Hu et al. [40] After deposition, the rGO coated Cu (Cu/rGO) electrodes were washed vigorously with DI water and dried under Ar flow. The Cu/PVP cathodes were fabricated by spin coating (500 rpm for the first 30 s and 2000 rpm for the next 30 s) of ethanolic PVP solution (7 wt%) over Cu foils. The PVP films casted over Cu foils were dried overnight at room temperature (25 °C). The same procedure was adapted to coat PVP layers over the prefabricated Cu/rGO substrates to obtain Cu/rGO/PVP electrodes (cathodes). The spin coating technique was also utilized to fabricate Nafion layer over the pre-fabricated Cu/rGO/PVP electrodes, i.e. to fabricate Cu/rGO/PVP/-Nafion hybrid electrodes. PVP and Nafion solutions of different concentrations (wt%) were utilized to obtain corresponding films of different thickness. As can be seen in Figs. S17 and S18 of the Supporting Information (SI), the electrochemical impedance spectroscopy (EIS) results of the films fabricated using 7 wt% PVP solution and 20 wt% Nafion solution produced Nyquist plots of lowest impedance values, indicating their lower energy barriers, and hence high charge transfer behaviors. The whole process of fabrication of the multi-layered hybrid composite cathode structure has been schematically depicted in Fig. S19 (Supporting Information) and physical properties of the prepared Cu/rGO/PVP/Nafion electrode are presented in Fig. S20 (Supporting Information).

All the four kinds of cathodes (Cu, Cu/rGO, Cu/rGO/PVP, and Cu/rGO/PVP/Nafion) were utilized for CO_2 reduction reactions to identify the function of each component layer (rGO, PVP and Nafion) in CO_2 reduction process.

2.3. Characterizations

2.3.1. Structural & morphological study

For structural analysis, powder X-ray diffraction (XRD) patterns of the fabricated photoanode and cathodes were recorded in a Rigaku D/MAX-2500/pc diffractometer, using CuKα ($\lambda = 1.5406$ Å) radiation. Surface morphology of the as-prepared CFO, TiO_2 and TiO_2:Ca-Fe samples was analyzed in a JEOL, JSM-7600 F field emission scanning electron microscope (FE-SEM), equipped with energy dispersive spectroscopy (EDS) analysis facility (X-Max). A JEOL JEM 2100 F transmission electron microscope (TEM) was utilized to obtain low and high resolution TEM (HR-TEM) images of the prepared CFO nanoparticles.

2.3.2. Spectroscopic analysis

A Varian Carry 5000 UV–visible-NIR spectrophotometer was utilized to obtain the diffuse reflectance spectra (DRS) of the electrode materials (TiO_2, TiO_2:Ca-Fe, rGO). Presence of rGO, PVP and Nafion in the fabricated multi-layered hybrid cathode was confirmed by infrared (IR) spectroscopy (Nicolate Avatar 330).

A Thermo VG Scientific Multitab 2000 X-ray photoelectron spectrometer (XPS) with Al K_α (1486.6 eV) X-ray source was utilized to analyze surface composition and chemical state of the elements in the TiO_2:Ca-Fe photoanodes prepared at 900 °C, 1000 °C and 1100 °C.

Room temperature time-resolved photoluminescence (TR-PL) spectra and images of the samples were recorded in a Hitachi F-7000 spectrophotometer attached with a confocal microscope (MicroTime-200, Picoquant, Germany). A single-mode pulsed diode laser (379 nm, 30 ps pulse width, ~10 μW power) was used as excitation source. A dichroic mirror (Z375RDC, AHF), a long-pass filter (HQ405lp, AHF), a 150 μm pinhole, and an avalanche photodiode detector (PDM series, MPD) were utilized to collect the emission from the samples. Exponential fitting of the experimentally obtained decay curves was performed through iterative least-square deconvolution, using Symphotime-64 software (Version 2.2).

2.3.3. Electrochemical characterization of photoanode

Linear sweep voltammetry (LSV), incident photon to converted electron (IPCE) efficiency, applied bias photon-to-current efficiency (ABPE), chronoamperometry, Mott-Schottky plot, impedance and open circuit potential (OCP) measurements were performed to study the electrochemical behavior of the fabricated TiO_2:Ca-Fe photoanodes. Photoelectrochemical measurements were performed in a three-electrode cell system using 0.1 M NaOH (pH ≈ 12.5) as electrolyte, Ag/AgCl in saturated KCl solution as reference electrode, TiO_2:Ca-Fe film as photoanode and a Pt plate as counter electrode. The photoanodes were irradiated by a simulated light source (solar simulator HAL-320, 300 W Xenon lamp) at AM-1.5 (1 sun) condition, utilizing a KG3 filter (3 mm, Schott).

2.3.4. Electrochemical characterization of the fabricated cathodes

The reaction cell (AP cell) utilized for electrochemical and photoelectrochemical studies consists of two compartments separated by Nafion membrane. While each of the compartments were of 20 cm^3 volume, we used 15 mL 0.1 M CO_2 saturated NaOH solution in each compartment. Both the electrodes (photoanode and cathode) were of 2 × 2 cm^2 dimensions. However, the effective area (area in contact with the electrolyte) of each electrode was about 1.13 cm^2. To estimate the reduction reaction overpotential of CO_2 molecule, acquired LSV data were plotted as potential (v) vs log (*j*) to obtain Tafel plots, where v is the applied bias potential and *j* is the photocurrent density. For collecting the LSV data, an AP cell containing TiO_2:Ca-Fe photoanode, Cu based multi-layered cathode, Ag/AgCl reference electrode, and 0.1 M NaOH aqueous electrolyte solution were utilized. Before collecting the data, CO_2 was purged in the electrolyte until its pH becomes stable, and the CO_2 gas was continuously purged during experiments. The pH of the CO_2 purged electrolyte was ~7.0, i.e. near neutral. Therefore, it is very unlikely to occur any homogeneous reaction including the reaction of CO_2 with the electrolyte. For the estimation of activation energy of $CO_2^{-\bullet}$ radical formation, electrochemical impedance spectroscopy (EIS) was performed over Cu cathode with and without PVP layer at different temperatures, replacing the TiO_2:Ca-Fe photoanode by Pt. The experiments were performed under −0.6 V (vs Ag/AgCl) external bias potential, in 100–0.010 Hz frequency range. Time-resolved chronoamperometry was utilized to verify the multi-electron transfer process through the rGO layer of the multi-layered hybrid cathode. For that purpose, a gold ultra-microelectrode tip coated with rGO was utilized as cathode, substituting the Cu based multi-layered cathode of the previous EIS experiment. Time-resolved chronoamperometry experiments were carried out with two step potential, in first step zero potential applied with respect to open circuit potential and in second step −0.6 V vs Ag/AgCl. Electron transfer rate was monitored for 200 μs under the same experimental conditions (Pt as anode, rGO-coated gold tip as cathode, Ag/AgCl reference electrode, 0.1 M NaOH solution electrolyte, −0.6 V external bias potential) under continuous CO_2 purging in the electrolyte solution. For comparison, the same experiment was repeated by coating the gold ultra-microelectrode cathode with known one-electron transfer media molecule of ethylphenothiazine (EPT) and two-electron transfer media molecule of N-ethyl-3,7-dimethoxyphenothiazine (DMeOEPT).

2.3.5. In situ spectroscopic analysis

To understand the CO_2 reduction pathway, electrochemical CO_2 reduction reactions were performed over pure Cu and Cu/PVP electrodes (cathodes) and monitored in situ by ATR-IR and Raman spectroscopies. *In situ* ATR-IR spectra of the electrode - electrolyte interface were recorded in a Thermo Scientific Nicolet 50 FT-IR spectrometer using a special horizontal ATR (HATR) cell accessory made by Pike technology, which includes a ZnSe crystal reflector of 4 mm thickness, and 7 × 0.9 cm^2 area. For in situ measurement, the ATR cell was filled with 0.1 M NaOH solution and purged with CO_2 gas for 60 min before recording IR spectra, and maintained throughout the measurement. The working electrodes (pure Cu or Cu/PVP) of same size (7 ×0.9 cm^2) were mounted on the HATR cell with active surface facing towards the ZnSe crystal. A Pt coil was used as counter electrode and Ag/AgCl as reference electrode. The CO_2 reduction reaction was carried out at − 0.68 V applied bias potential and the spectra were recorded at every 10 sec interval for 1 h reaction time.

In situ Raman measurements were performed in a Nanobase Xperam-F1.4 spectrometer equipped with 785 nm microprobe laser of 200 mW power. The electrochemical conditions used for in situ ATR-IR study were the same as used for in situ Raman measurements.

To confirm the formation of CO_2 anion radicals ($CO_2^{-\bullet}$) as the first intermediate of CO_2 reduction reaction, electron paramagnetic resonance (EPR) spectroscopy at low temperature (5.0 K) was performed on the phenyl-N-tert-butylnitrone (PBN, 0.1 M) entrapped electrolyte aliquots collected during the CO_2 reduction reaction. A Bruker EMX/Plus spectrometer with dual mode cavity (ER 4116DM) was utilized for this purpose. For recording the EPR signals, the microwave frequency, modulation frequency, and microwave power were set as 9.64 GHz, 100 kHz, and 0.94 mW, respectively. CO_2 reduction reactions were performed in 20 mL electrolyte made of equimolar PBN (0.1 M) and CO_2 saturated NaOH (0.1 M) solutions, utilizing Cu/rGO/PVP/Nafion hybrid composite cathode and TiO_2:Ca-Fe photoanode, under 0.68 V bias (vs RHE) potential and one-sun solar light illumination of the photoanode. After 20 min of reaction, about 100 μL electrolyte solution was collected from the electrochemical cell, transferred to the quartz tube EPR sample holder, and frozen in liquid nitrogen immediately. EPR analysis of the collected sample was performed near liquid helium (5.0 K) temperature.

2.4. Photoelectrochemical CO_2 reduction

Photoelectrochemical CO_2 reduction reactions were carried out in an

air-tight glass-made continuous flow reactor, consisting of Nafion membrane separated anodic and cathodic compartments and quartz windows. TiO_2:Ca-Fe film photoanode of about 1.13 cm^2 surface area, multi-layered hybrid cathode of same surface area (1.13 cm^2), and a Ag/AgCl reference electrode (in 3 M KCl solution) were utilized in a three electrode system. Before performing the CO_2 reduction reaction, both the anode and cathode compartments were filled with 20 mL (in each compartment) of 0.1 M NaOH aqueous electrolyte solution and purged with CO_2 gas for 30 min. Photoelectrochemical CO_2 reduction was carried out for 2, 4, and 8 h under AM-1.5 solar simulated radiation (HAL-302 Asahi) of 100 mW cm^{-2} power, which is approximately equivalent to 1 sun. After each reaction, about 10 mL of electrolyte solution was collected from the electrochemical cell for GC analysis of the products. The headspace of the used GC system can carry the sample containing air-tight glass bottle and inject the sample into GC automatically through solid phase micro-emulsion (SPME) system. The contents of formaldehyde and acetaldehyde in the electrolyte solution were estimated in μM per unit area (μM cm^{-2}) by the flame ionization detector (FID, with attached molecular sieve column) of the GC, using the reference calibration curves of formaldehyde and acetaldehyde prepared using their aqueous solutions of known concentrations in the same GC system (Figs. S21 and S22, SI). All the tests have been performed at least five times under similar experimental conditions using separate composite cathodes.

3. Results and discussion

In this section work has divided into two part such as, anodic compartment and cathodic compartment. The cathodic compartment further divided into four subsections as follows, (i) CO_2 capture and activation, (ii) multi electron shuttling, (iii) reduction potential tuning and (iv) CO_2 reduction by electron-coupled proton transfer process.

3.1. Anodic compartment: Ca, Fe doped TiO_2 photoanode

Structural and morphological characteristics of the synthesized calcium ferrite (CFO) particles and fabricated TiO_2:Ca-Fe photoanodes are presented in Figs. S1 & S2 (Supporting Information, SI), respectively. As can be seen, the photoanode fabricated by air-annealing of CFO-covered Ti foil at 1000 °C consists of well-crystalline titania particles of rutile phase. Incorporation of Ca and Fe in the TiO_2 films over the Ti foils through thermal-diffusion from the attached CFO particles during high temperature air-annealing is clear in the X-ray photoelectron spectra (XPS) of the photoanodes presented in Fig. S3 (SI). Incorporation of Ca and Fe atoms in the lattice reduced the band gap energy of rutile TiO_2 [41,42] (Fig. S4, SI), enhancing the activity of photoanodes under visible light irradiation (Fig. S5, SI). As expected, the TiO_2:Ca-Fe photoanodes fabricated by air-annealing at 1000 °C revealed best visible-light PEC response among all the fabricated photoanodes prepared by annealing at higher (1100 °C) or lower (900 °C) temperatures. As can be seen, the photoanodes fabricated at this annealing temperature are highly stable until 50 h of reaction time (Fig. S6, SI). PEC reduction of CO_2 was carried out for different reaction times (2, 4 and 8 h) under different applied bias potentials (0.28, 0.48, 0.68, 0.88 and 1.18 V vs RHE). The amount of CO_2 reduction liquid products (formaldehyde and acetaldehyde) was seen to increase with reaction time (although not linearly due to the formation of gas bubbles over the electrodes) for all the fabricated cathodes (Figs. S7 & S8, SI). To study the effect of external bias potential, CO_2 reduction experiments were carried out for 8 h.

3.2. Cathodic compartment: Nafion/PVP/rGO/Cu cathode

Utilizing TiO_2:Ca-Fe photoanode, CO_2 reduction reactions were carried out for all the fabricated cathodes (Cu foil, Cu/rGO, Cu/rGO/PVP, Cu/rGO/PVP/Nafion). On utilizing pure Cu foil as cathode, no liquid fuel was produced, indicating that a pure Cu foil cathode cannot reduce CO_2 to liquid fuel under the used experimental conditions. While the possibility of generating CO, HCOOH, C_2H_4 and CH_4 as CO_2 reduction product using metallic Cu cathode in electrochemical system has been predicted, [43] production of gaseous hydrocarbon fuels such as methane and ethylene through electrochemical reduction of CO_2 in aqueous $KHCO_3$ electrolyte using metal (including Cu) has been demonstrated by Hori et al. [44] The non-occurrence of any reduction product in the present case might be due to the use of different electrolyte (CO_2 saturated 0.1 M NaOH solution). In fact, different electrolytes create different environments for CO_2 adsorption and generate different reaction products. The PEC system used in this study consisted of TiO_2:Ca-Fe photoanode, CO_2 saturated 0.1 M NaOH solution electrolyte, and bare Cu foil cathode. Even though the Cu foil cathode can adsorb a few CO_2 molecules (purged during the reaction) on the surface, due to the high reduction potential and high activation energy, complete reduction of CO_2 molecule is almost impossible at room temperature.

On the other hand, utilization of Cu/rGO cathode did induce (Fig. 1a) CO_2 reduction reaction, generating formaldehyde as the only product for the whole (0.2–1.2 V) applied bias potential range. As can be noticed, for a fixed period of reduction reaction (8 h in the present case), the amount of generated formaldehyde strongly depends on the value of applied bias potential. Optimum bias potential for formaldehyde generation was seen to be around 0.68 V (vs RHE), which produced approximately 470 μM of formaldehyde in 8 h.

Utilization of Cu/PVP and Cu/PVP/Nafion cathodes resulted in the formation of both formaldehyde and acetaldehyde (see Fig. S8, SI). As can be noticed in Fig. 1b, the amount of generated formaldehyde and acetaldehyde over Cu/PVP cathode varies almost inversely with applied bias potential. While at lowest applied bias potential (0.2 V vs RHE) the fraction of generated formaldehyde is about 80% (in molar term) of the total products, at the highest applied bias potential (1.2 V vs RHE) it is only about 24% of the total products, clearly demonstrating the bias potential dependence of reaction pathways in the multi-step CO_2 reduction process. However, on utilizing Cu/PVP/Nafion multi-layer hybrid composite as cathode (Fig. 1c), while the formaldehyde yield varied with bias potential in the same manner as in the case of Cu/rGO cathode, the acetaldehyde yield increased steadily until 0.88 V (vs RHE) of bias potential and then decreased. It must be noted that the maximum amount of formaldehyde generated in the latter two cases are considerably less than that produced over Cu/rGO cathode. Even by considering the amounts of both the reaction products (i.e. formaldehyde and acetaldehyde), the total amounts of generated products in the latter two cases were substantially less than the amount of formaldehyde produced by Cu/rGO cathode at optimum bias potential, demonstrating a large electron accumulation capacity of rGO in the multi-layer cathode.

Finally, the utilization of Cu/rGO/PVP/Nafion multi-layered hybrid composite cathode produced only acetaldehyde as CO_2 reduction product for the whole range of applied bias potential (Fig. 1d). At optimum bias potential of 0.68 V (vs RHE), a maximum ~ 450 μM of acetaldehyde was produced during 8 h of reaction. The results presented in Fig. 1(a'-d') reveal that formaldehyde (~ 470 μM in 8 h) is the major product over Cu/rGO cathode with 25% current efficiency and acetaldehyde (~ 450 μM in 8 h) is the major product over Cu/rGO/PVP/Nafion cathode with 39% current efficiency for photoelectrochemical reaction of CO_2 at 0.68 V (vs RHE) bias potential. In the case of other two cathodes (i.e. Cu/PVP and Cu/PVP/Nafion), both formaldehyde and acetaldehyde were produced with varied current efficiencies for different applied bias potentials. The results also indicate that while 0.68 V (vs RHE) is the optimum bias potential for the Cu/rGO/PVP/Nafion cathode, it (optimum bias potential) depends on the constituents/composition of the hybrid cathode. While the product efficiency of each liquid fuel is optimum for specific bias potentials, in general, a lower bias potential is preferred energetically.

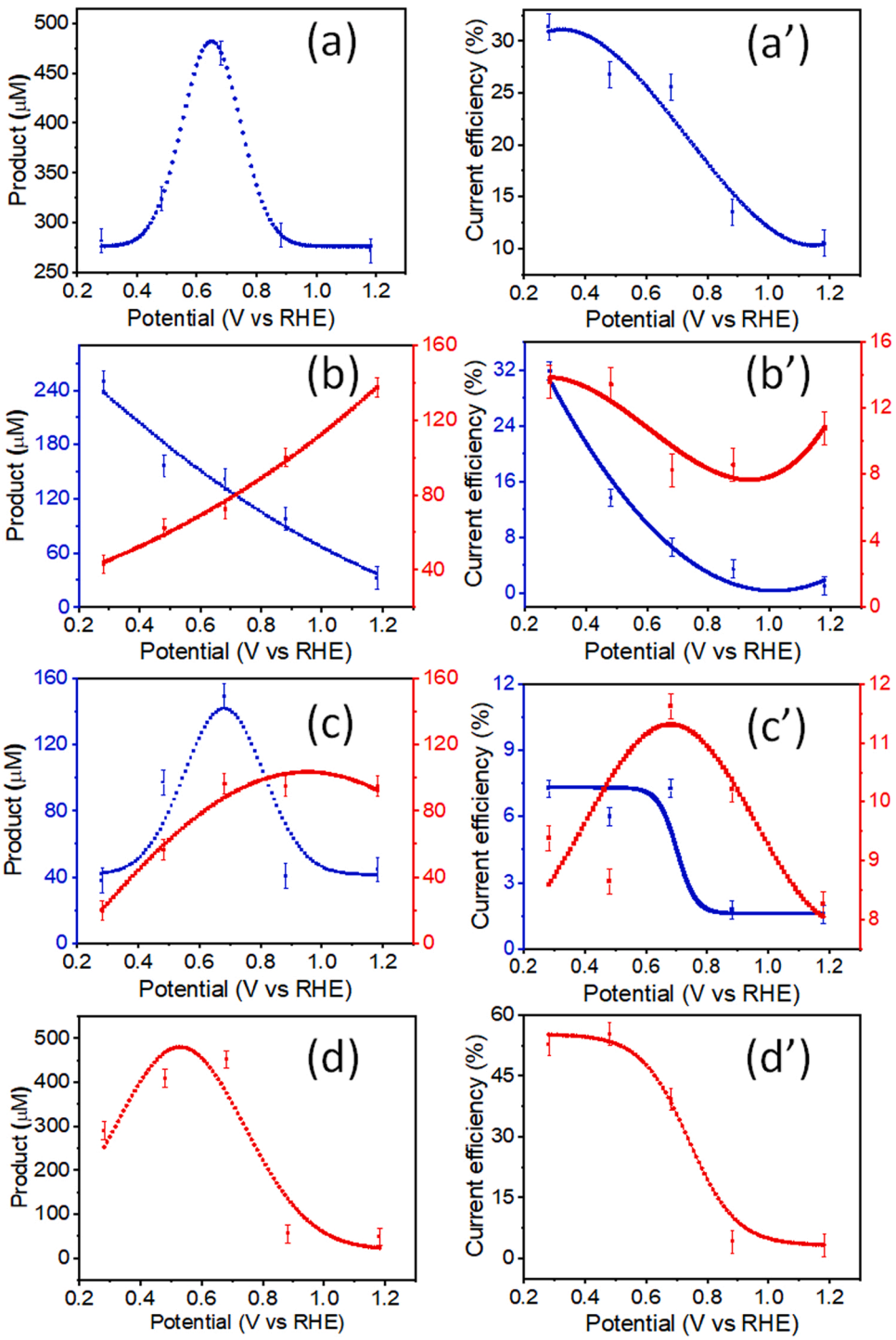

Fig. 1. Quantitative analyses and current efficiency of CO_2 reduction products. Bias potential dependent CO_2 reduction products and corresponding current efficiencies on (a, a′) Cu/rGO, (b, b′) Cu/PVP, (c, c′) Cu/PVP/Nafion, and (d, d′) Cu/rGO/PVP/Nafion hybrid cathode. TiO_2: Ca-Fe film was utilized as photoanode. Formaldehyde and acetaldehyde yields are plotted in blue and red color, respectively. Error bars in the plots represent CI of the data values. (For interpretation of the references to color in this figure legend, the reader is referred to the web version of this article.)

3.2.1. CO_2 capturing and activation (through PVP)

A reduction in energy difference between the ground state of CO_2 and its first activated state is expected to enhance the reaction kinetics and decrease the CO_2 reduction energy of electron transfer from cathode to CO_2 molecules. Presence of PVP in the hybrid composite cathode not only reduces the reaction overpotential through activation of CO_2 molecules by complexing with PVP as stated earlier, but also provides a larger number of active sites at cathode surface for CO_2 capture, making the CO_2 reduction process more efficient. Fig. 2 (a–c) shows the comparative Tafel plots of pure Cu, Cu/PVP and Cu/rGO/PVP/Nafion composite electrodes used for the estimation of reaction overpotentials for the three cases. The pure Cu electrode revealed an overpotential value of 11.46 KJ/mol, which is relatively larger than the values obtained for Cu/PVP (6.16 KJ/mol), and Cu/rGO/PVP/Nafion (9.00 KJ/mol) electrodes. As has been stated earlier, a decrease in reaction overpotential decreases the CO_2 reduction energy. Considering both the CO_2 reduction reaction overpotential (Fig. 2 (a–c)) and activation energy for CO_2 anion radical ($CO_2^{-\bullet}$) formation as rate determining step of CO_2 reduction reaction (Fig. 2 d), we present the schematics of step-wise energy transfer processes involved in the CO_2 reduction process over Cu/PVP and Cu/rGO/PVP/Nafion hybrid composite electrodes in comparison with pure Cu electrode (Fig. 2 (e–f)). The activation energy of CO_2 reduction reaction (activation overpotential) could be estimated considering the energy of the activated CO_2 molecule in reactant state

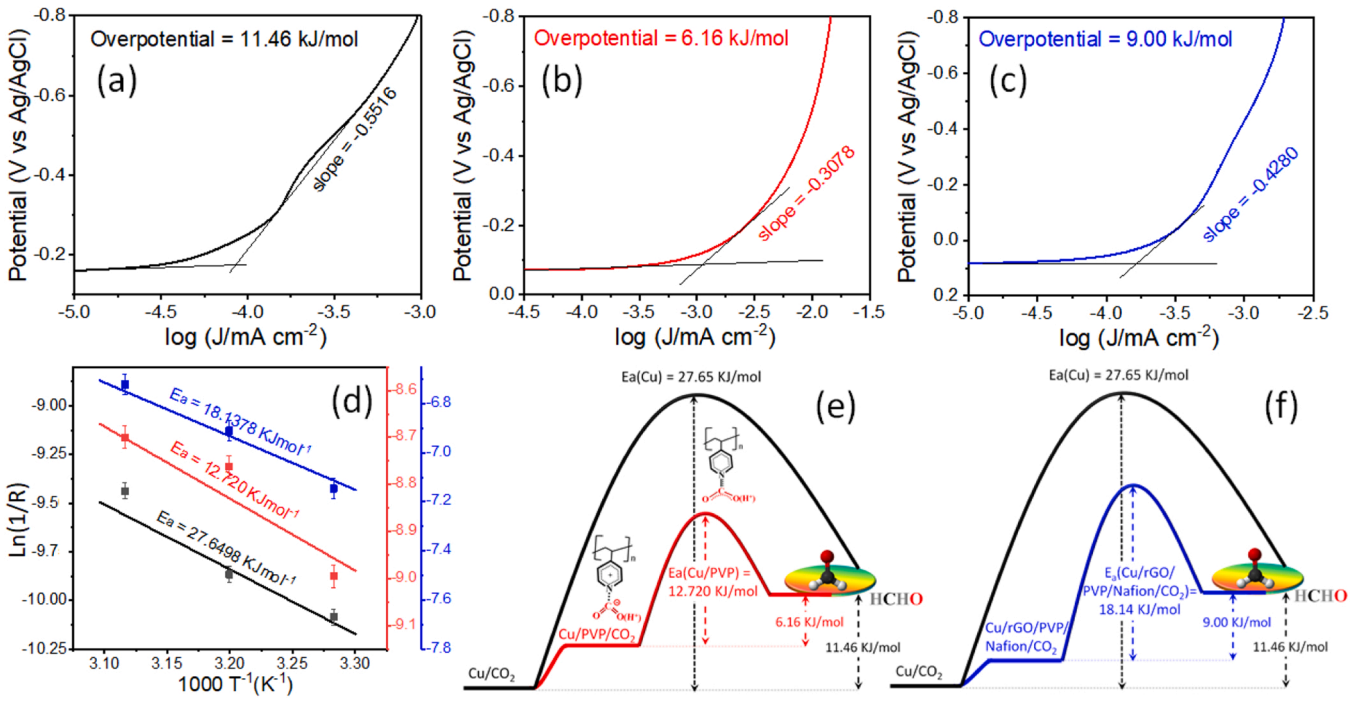

Fig. 2. Reaction overpotential and activation energy estimation from Tafel plots and temperature dependent EIS Nyquist plots. Estimation of CO_2 reduction overpotential from Tafel plot of (a) pure Cu, (b) Cu/PVP and (c) Cu/rGO/PVP/Nafion hybrid cathode. (d) Arrhenius plots for the estimation of activation energy of CO_2 reduction to $CO_2^{-\bullet}$ anion radical (the first intermediate of CO_2 reduction reaction) from temperature dependent EIS, of respective cathode electrodes. (e) Schematic energy level diagram showing CO_2 reduction pathway for pure Cu (black) and Cu/PVP (red) cathode electrodes. (f) Schematic energy level diagram showing CO_2 reduction pathway for pure Cu (black) and Cu/rGO/PVP/Nafion (blue) cathodes. (For interpretation of the references to color in this figure legend, the reader is referred to the web version of this article.)

and the change in transition state energy barrier (height) for the electron transfer to CO_2 molecules as shown in Fig. 2e & f.

As can be noticed, for the Cu/PVP cathode (Fig. 2e), the activation energy of CO_2 reduction reaction is lower than for Cu/rGO/PVP/Nafion cathode (Fig. 2f). Incorporation of rGO and Nafion in cathode slows down the electron transfer kinetics due to larger activation energy; resulting in a longer life-time of intermediate $CO_2^{-\bullet}$ radical. This allows the dimerization of $CO_2^{-\bullet}$ radical into acetaldehyde as has been

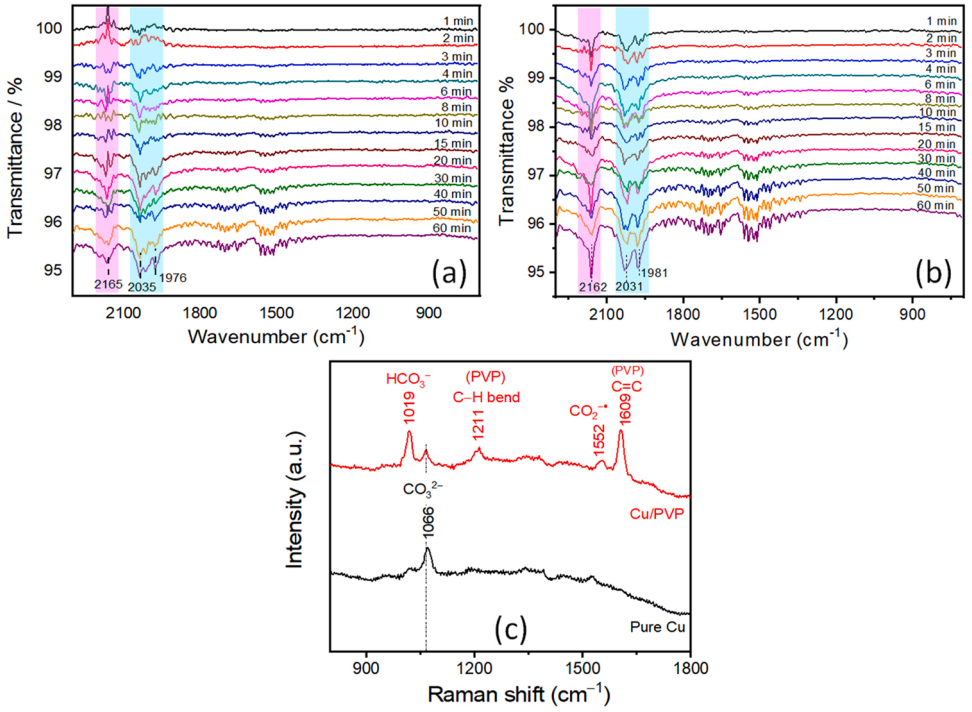

Fig. 3. *In situ* monitoring of role of PVP in CO_2 reduction. ATR-IR spectra of (a) pure Cu, and (b) Cu/PVP electrode – electrolyte interfaces, during CO_2 reduction. (c) Typical in situ Raman spectra of the electrodes during CO_2 reduction.

indicated in our proposed mechanism presented in Fig. S13 (Supporting Information). The rGO and Nafion layers enhance the multi-electron transfer (from cathode surface) and multi-proton transfer (from the electrolyte) rates towards the intermediates at CO_2 reduction sites, respectively, facilitating the production of acetaldehyde through dimerization of $CO_2^{-\bullet}$ radicals. This allows the product selectivity change from formaldehyde (which is a 4-electron and 4-proton) to generate acetaldehyde (10-electron and 10-proton) (see Fig. 1d).

To study the role of PVP layer in the fabricated multi-layered hybrid composite cathode, we performed in situ ATR-IR and in situ Raman studies of the functional PVP layer at the cathode-electrolyte interface during CO_2 reduction reaction under the conditions identical to that used for CO_2 reduction process. As can be seen in Fig. 3, both the pure Cu and Cu/PVP electrode revealed IR absorption bands, one peaked around 2165 cm^{-1} and others located in-between 2031 and 1976 cm^{-1}. While the IR band located around 2165 cm^{-1} has been attributed to free (released) CO molecules, the bands appeared in 2031 – 1976 cm^{-1} spectral range have been attributed to adsorbed CO molecules [45,46]. However, the intensity of both the IR bands (adsorbed and released) was much higher for the Cu/PVP electrode than that of the bare Cu electrode, indicating its enhanced CO_2 capturing ability. On the other hand, in situ Raman spectra of the electrodes (Fig. 3c) revealed distinct dispersion features. While the Raman spectrum of the bare Cu electrode revealed only one dispersion band around 1066 cm^{-1} related to CO_3^{2-} ion formed due to deprotonation of bicarbonate ($HCO_3^- \rightarrow H^+ + CO_3^{2-}$) [47] in the electrolyte solution (0.1 M $NaHCO_3$), the spectrum for the Cu/PVP electrode revealed four additional dispersion bands around 1019, 1211, 1552 and 1609 cm^{-1}. The peaks appeared around 1609 and 1552 cm^{-1} correspond to the ν_1 and ν_2 stretching modes of C=C bond of pyridine ring, the peak revealed at 1211 cm^{-1} corresponds to in-plane bending mode of C-H bond in PVP [48]. Finally, the dispersion band appeared around 1019 cm^{-1} corresponds to HCO_3^- ion generated in the electrolyte [49]. As can be noticed in Fig. S11 (Supporting Information), the intensity of the dispersion peak at 1552 cm^{-1} increased on applying bias potential (−0.68 V). Such intensity enhancement of the 1552 cm^{-1} band for the biased case might be the result of superposition of dispersion band of $CO_2^{-\bullet}$ radicals (attached to the PVP layer) with the C=C stretching mode of pyridine ring of PVP. While the Raman dispersion band of $CO_2^{-\bullet}$ radicals attached to Cu substrate has been seen to appear in 1520–1540 cm^{-1} spectral range [47], a shift in position of the dispersion band cannot be discarded as the substrate in the present case is different (PVP).

3.2.2. *Multi-electron shuttling (through rGO)*

The electron scavenging and transfer (to CO_2 molecules adsorbed over the cathode surface) characteristics of rGO were monitored by recording time-resolved chronoamperometric traces of the cathodes fabricated by rGO coating over Au ultra-microelectrodes. A Pt coil and standard Ag/AgCl (in KCl solution) were used as counter and reference electrode, respectively, for this purpose. For comparison, time-resolve chronoamperometric traces were also recorded for the working electrodes fabricated by dip coating of standard one-electron and two-electron transfer media molecules such as ethylphenothiazine (EPT) and N-ethyl-3,7-dimethoxyphenothiazine (DMeOEPT), respectively, over the Au ultra-microelectrode. All the experiments were performed in 0.1 M NaOH electrolyte after 30 min of CO_2 purging. The electron transfer processes in the materials are presented schematically in Fig. 4 (a–c), along with their time-resolved chronoamperometric traces (Fig. 4d). Estimated areas under the TR-chrono traces (for a fixed decay time) of the three materials as electron donor (EPT, DMeOEPT, and rGO) were approximately in 1:2:4 ratio, demonstrating not only the electron capturing behavior of rGO through non-Faradaic process, but also its involvement in the four-electron transfer process during CO_2 reduction into formaldehyde. To verify the electron capturing and accumulating

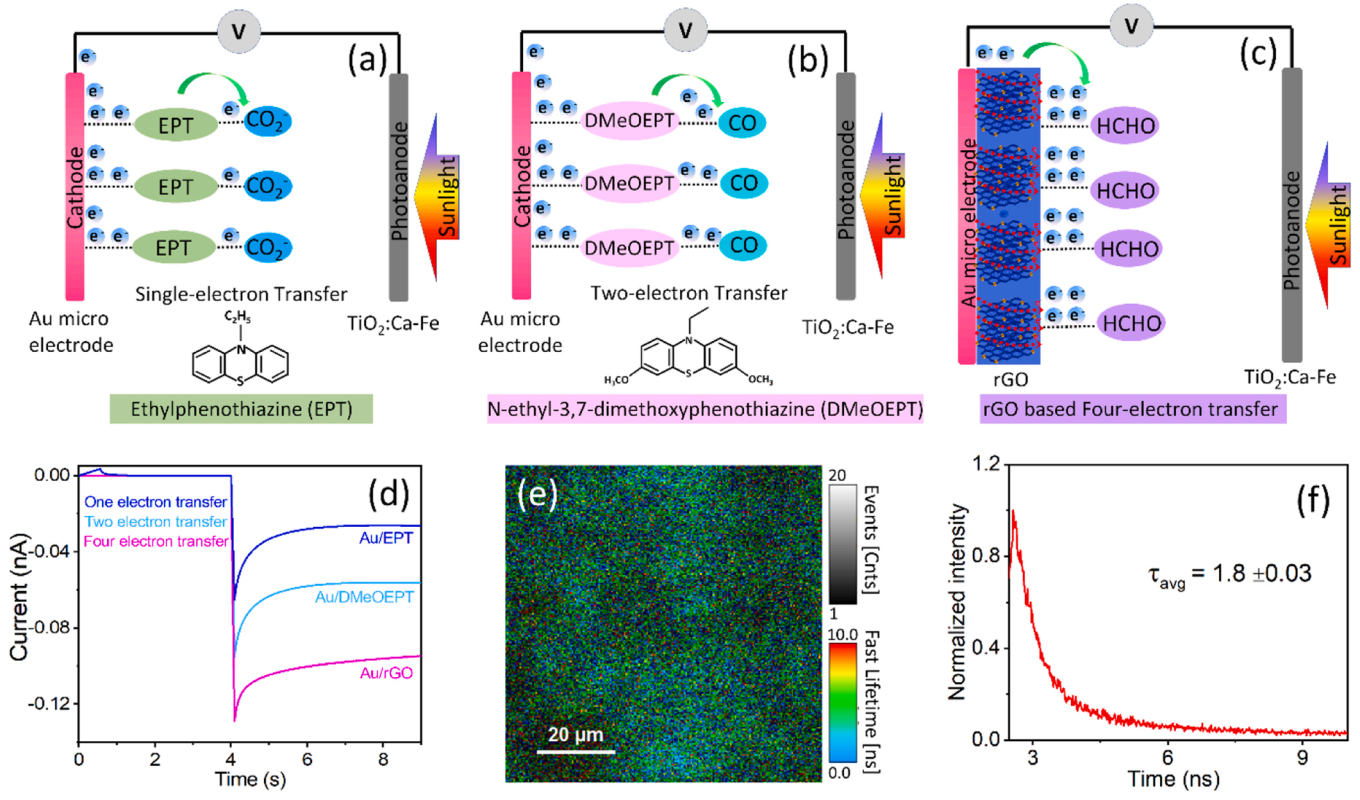

Fig. 4. TR-chronoamperometry and time-resolved PL characteristics of Cu/rGO electrode. Schematic presentation of (a) one-electron transfer, (b) two-electron transfer, and (c) four-electron transfer process induced by EPT, DMeOEPT, and rGO, respectively. TR-chronoamperometric traces for these three materials are presented in (d). Typical (e) 2D TR- PL image and (f) luminescence decay curve of rGO coated Cu electrode.

behaviors of rGO in the multi-layered cathode and its contribution in CO_2 reduction process, 2D electron density mapping image and time-resolved photoluminescence (TR-PL) decay measurements were performed on pure and rGO coated Cu foils, exciting them by a 375 nm single-mode pulsed diode laser beam (< 1 μW power, 240 ps pulse duration, 10 MHz repetition frequency) at room temperature. A TR-PL system coupled with an inverted-type scanning confocal microscope (Picoquant Micro Time-200) was utilized for the analysis. As can be seen in Fig. 4e, the density of excited electrons at the surface of rGO-coated Cu foil is considerably higher than that at the surface of pure Cu foil (Fig. S10b, SI), clearly demonstrating the excellent electron capturing and accumulating ability of the rGO layer. On the other hand, estimated life-time of excited electrons for the rGO-coated Cu foil (extracted by exponential fitting of the TR-PL curves, Fig. 4f) sample was ~1.8 ns, while it was about 0.9 ns for the pure Cu foil (Fig. S10c, SI). About two order longer carrier life-time for the rGO-coated Cu foil clearly demonstrates the role of rGO in the Cu/rGO/PVP/Nafion hybrid composite cathode for the enhancement of non-Faradaic electron accumulation for the electrocatalytic CO_2 reduction process. In fact, such a longer life-time of the excited (free) electrons at cathode surface facilitates the multi-electron shuttling process involved in PEC CO_2 reduction reaction. The electrons collected at the cathode surface (accumulated over rGO layer) are transported to CO_2 molecules adsorbed (and activated) over the PVP layer of the multi-layered cathode.

3.2.3. *Reduction potential tunning (through external bias)*

As reduction overpotential is the amount of thermodynamic energy required for complete reduction of a reactant to obtain the reaction product, a variation in CO_2 reduction overpotential would also result in the formation of different hydrocarbon products. On the other hand, reduction potential of CO_2 in an electrochemical environment is function of several parameters such as the nature of electrode material, pH of the electrolyte, temperature and pressure of the reaction ambient. Therefore, estimation of CO_2 reduction potential in EC or PEC system is a trivial task. In fact, using different EC or PEC set-ups, different research groups have reported on CO_2 reduction potential values considering only the pH of their used electrolytes [50]. Here by considering the electronic properties of active materials of multi-layered cathode and photoanode, along with open circuit potential of the PEC cell (which depends also on the pH of the used electrolyte), we demonstrate that by tuning external bias potential it is possible to control the energy of CO_2 reduction to generate fuel products selectively.

For this purpose, we considered the following four parameters: (1) open circuit potential (V_{oc}) of the cell, (2) conduction band position of the photoanode (V_a), (3) conduction band position of cathode (V_c), and (4) applied external bias potential (V_b). Conduction band positions of the photoanode and cathode were estimated from their valence band positions and band gap energies estimated from ultraviolet photoelectron spectroscopy (UPS) analysis and Kubelka–Munk (K-M) plots (Fig. S14, SI), respectively. The energy band diagrams of the photoanode and cathode in the PEC cell drawn by considering the above parameters have been schematically depicted in Fig. 5. On irradiating the photoanode by solar light (step 1, Fig. 5), the electrons of its valence band (VB) get excited to its conduction band (step 2, Fig. 5), acquiring a potential energy V_a ($V_a = 0.22$ V vs RHE) from solar light. However, this energy of the photoexcited electrons is not enough to reach the cathode through external circuit by itself as the conduction band (CB) of Cu/rGO at cathode lies above the CB of TiO_2:Ca-Fe photoanode, or the potential energy (V_a) of the photoexcited electrons. Therefore, it is necessary to apply an external bias potential (V_b) to transport the photoexcited electrons to the dark cathode. On application of external bias potential, the net potential difference between the photoanode and cathode becomes V_{eff} ($V_{eff} = V_{oc} - V_b + V_a$) (step 3, Fig. 5), under which the electrons at the CB of photoanode move towards the cathode. On reaching the CB of cathode, the electrons acquire a total energy of $V_{tot} = V_{eff} + V_c$ (step 4, Fig. 5), with which they will be used to reduce CO_2 by interacting with the CO_2 molecules on the cathode surface. For the present experimental conditions, estimated V_{eff} and V_{tot} values of the electrons under different applied bias potentials are listed in Table S1 (SI). As has been stated earlier, reduction potentials of CO_2 for different obtaining different reduction products are different. When the external bias potential-tuned energy of the electrons at cathode surface matches with the reduction energy of CO_2 for a selected reduction product, we obtain the product fuel as the reduction product selectively.

As can be noticed in Fig. 5, for an external bias potential (V_b) of 0.68 V (vs RHE), the V_{tot} of the electrons is about −0.064 V, which is very close to the reduction reaction potential value (−0.0663 eV, Table S1, SI) of CO_2 for formaldehyde (HCHO) production. On the other hand, acetaldehyde is a dimerized product of carboxyl radical, which can be generated along with formaldehyde during CO_2 reduction with excess supply of electrons at the cathode surface, as has been discussed earlier. While the reduction of CO_2 to formaldehyde is a 4-electron and

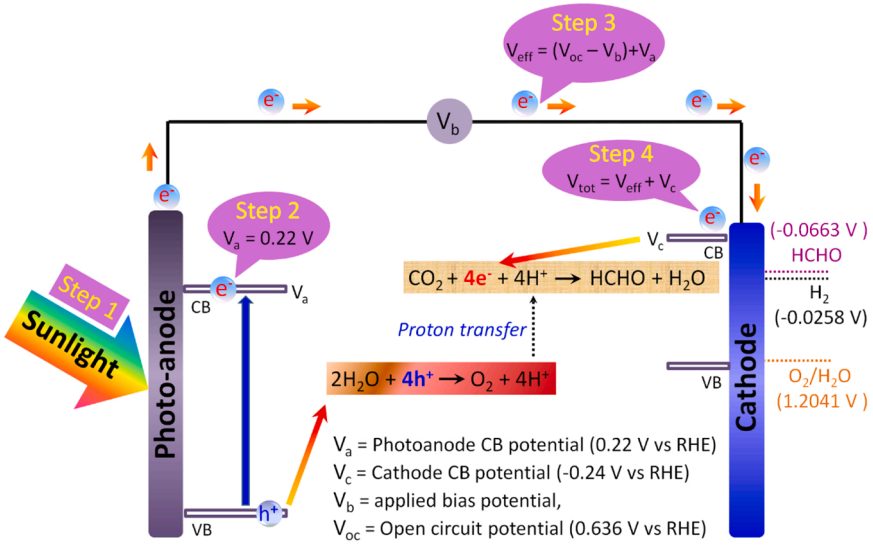

Fig. 5. Bias potential tuning for CO_2 reduction. Schematic presentation of energy level diagram of TiO_2:Ca-Fe photoanode and Cu/rGO cathode in a PEC cell (under CO_2 bubbling) and bias potential tuning. Variation of energy of the electrons generated at the photoanode under illumination at each of the 4 steps (photo-excitation, transition to the CB of semiconducting photoanode, application of external bias, and transportation to cathode) have been illustrated.

4-proton transfer process, reduction of CO_2 to acetaldehyde is 10-electron and 10-proton transfer process. Therefore, the production of acetaldehyde in the present case is critically controlled by two parameters: (1) the activation overpotential of electron transfer, which is reduced to be fast process by the PVP layer as activator, and (2) rate of multi-electron and multi-proton transfer at CO_2 reduction site, which depend on the electron accumulating plus conducting ability of rGO and proton conducting ability of the Nafion layer, respectively. With longer life-time of $CO_2^{-\bullet}$ anion radical due to high activation overpotential of electron transfer, large charge capacity of rGO layer and the good proton conducting ability of Nafion layer, generation of acetaldehyde is more probable at the surface of Cu/rGO/PVP/Nafion hybrid composite cathode than formaldehyde (see Fig. 1).

3.2.4. CO_2 reduction by sequential multiple electron-coupled proton transfer process

Finally complete CO_2 reduction process occurs due to the synergetic effects of electron accumulating ability of rGO for multi-electron shuttling function, CO_2 capturing and activating abilities of PVP, and proton transporting capacity of Nafion. The in detailed schematic illustration has presented in Fig. 6. Bias potential dependence of CO_2 reduction and protonation dynamics of $CO_2^{-\bullet}$ radicals are clearly reflected in the bias potential-dependent acetaldehyde yield presented in Fig. 1d. Used PEC set-up and different steps of the CO_2 reduction process have been depicted schematically in Fig. 6.

3.3. Tracing the CO_2 reduction process with ^{13}C-isotpe labeling study

To confirm that CO_2 is the only carbon source of the obtained reduction products (formaldehyde and acetaldehyde), we performed ^{13}C labeling experiments utilizing 0.1 M $NaH^{13}CO_3$ as electrolyte and $^{13}CO_2$ as the bubbling gas instead of CO_2 saturated 0.1 M NaOH electrolyte and normal CO_2. As can be seen in Fig. S9 (Supporting Information) the GC-MS spectra revealed two clear signals at $m/z = 30$ (with retention time 6.14) and 45 (with retention time 6.25) for all the hybrid cathodes except Cu/rGO, which correspond to formaldehyde and acetaldehyde, respectively. On the other hand, a blank test performed (not presented) in the same system without CO_2 purging revealed no GC-MS signal correspond to these two compounds. The results clearly demonstrate that CO_2 is the only carbon source for the generation of formaldehyde and acetaldehyde.

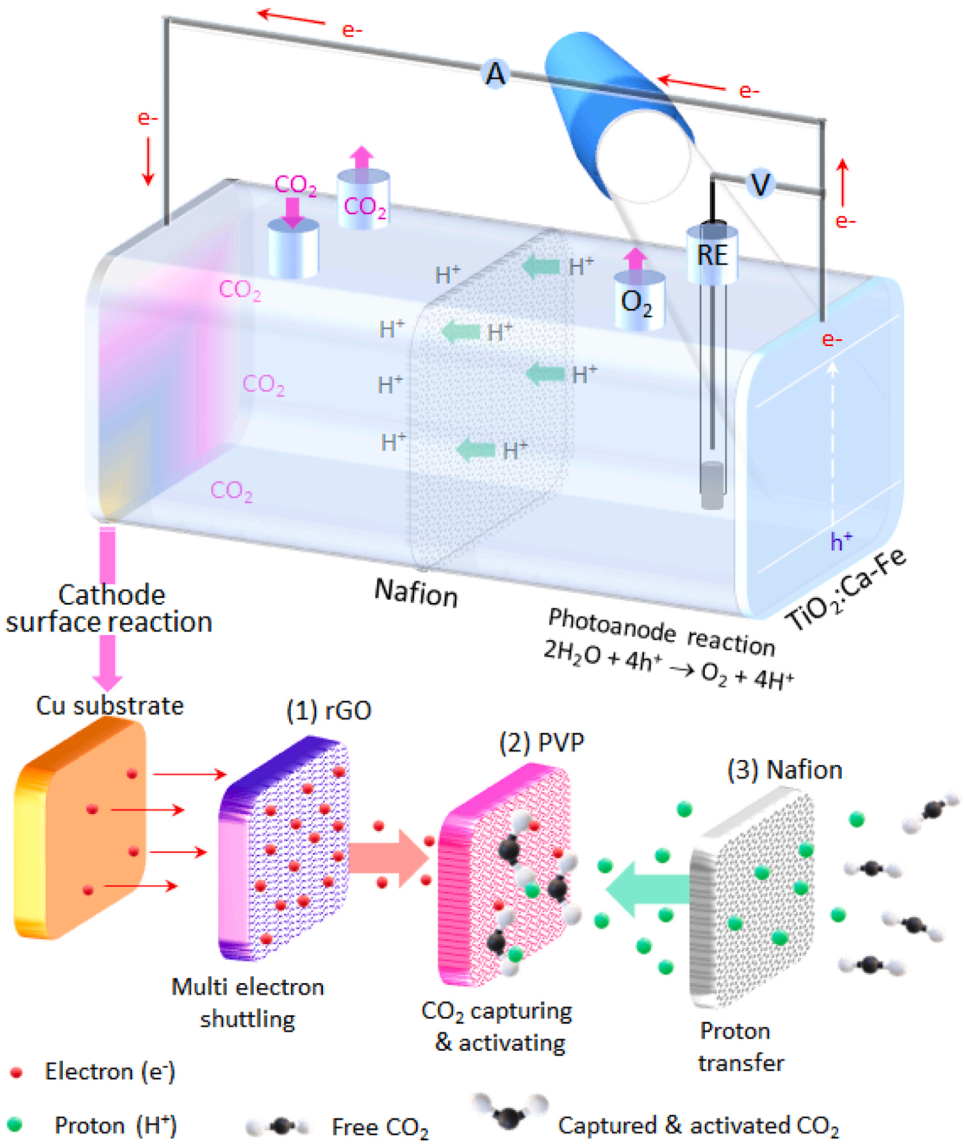

Fig. 6. Schematics of the used PEC cell and the CO_2 reduction process. Schematic presentation of PEC cell consisting Cu/rGO/PVP/Nafion multi-layered hybrid cathode and TiO_2:Ca-Fe photoanode utilized for CO_2 reduction (upper case), along with the involved CO_2 reduction steps. Step 1: accumulation of photoelectrons on rGO surface; step 2: captured and activation of CO_2 in PVP layer; Step 3: proton transfer (from the electrolyte to PVP layer) through Nafion; and finally formation of formaldehyde and acetaldehyde take place through proton coupled electron transfer at the PVP-nafion interface.

3.4. Further discussion

Formation of $CO_2^{-\bullet}$ radical intermediate during CO_2 reduction reaction was confirmed further by low temperature electron paramagnetic resonance (EPR) spectroscopy (Fig. S12, SI). As can be noticed in the simulated EPR spectrum presented in Fig. 7, the phenyl-N-tert-butylnitrone (PBN)-trapped reaction product (under CO_2 bubbling) revealed a triplet resonance band of $[CO_2{-}PBN]^{-\bullet}$ intermediate radical with g = 2.0052 [51] and coupling constant (A) = 55 G, clearly indicating the formation of $CO_2^{-\bullet}$ anion radical intermediate in the CO_2 reduction process. The small singlet band appeared in the EPR spectrum at g = 2.0679 corresponds to the $CO_3^{-\bullet}$ anion radicals formed due to the reaction of bicarbonate ions of the electrolyte with $OH^\bullet$ radicals formed during water reduction following the reaction $HCO_3^- + OH^\bullet \rightarrow CO_3^{-\bullet} + H_2O$ (see SI for details).

Finally, to evaluate the efficiency of the PEC process, we estimated the current efficiency (Faradaic efficiency) of CO_2 reduction reaction considering the principal reduction products, i.e. formaldehyde, acetaldehyde and H_2 obtained after 8 h of reaction. The current efficiency of the PEC CO_2 reduction process for Cu/rGO/PVP/Nafion hybrid composite cathode was estimated to be around 60% (Fig. S15,SI). On the other hand, the current efficiency estimated for 2 h of reduction under the same reaction conditions was much higher (**85%**). The observed energy loss, i.e., the lower current efficiency of the reduction process for longer reaction time is understandable if we analyze the GC spectra of the products presented in Fig. S7 (Supporting Information) carefully. As can be noticed, intensity of the GC signals corresponding to formaldehyde and acetaldehyde under 0.68 V (vs RHE) bias potential did not increase linearly with reaction time, indicating an increment of transport resistance due to the formation of gas bubbles over the surface of electrodes (due to water splitting) for longer reaction time [52]. Although a longer reaction time has not been considered normally for laboratory scale reactions, for commercial usage, we need to think for a solution of this problem, probably by considering rotating electrodes.

4. Conclusions

Utilizing Ca and Fe co-doped TiO_2 photoanode and Cu/rGO/PVP/Nafion multi-layered hybrid composite cathode, we demonstrate the generation of formaldehyde and acetaldehyde selectively through photoelectrochemical reduction of CO_2. While a photo-responsive semiconducting anode controls the energy of photo-excited electrons at its surface, in coordination with the proton conducting cathode, it determines the current density of the PEC cell. On the other hand, PVP and rGO layers of the cathode control the CO_2 capture and electron transfer rate (from cathode to CO_2 molecules), respectively. By monitoring the role of each of the components of the multi-layered cathode through TR-PL, TR-chronoamperometry, in situ ATR-IR, Raman, and EPR spectroscopies along with the kinetics of the reduction process, we could provide possible reaction pathways for the production of formaldehyde and acetaldehyde on the cathode surface. Moreover, by taking into account the characteristics of photoanode and dark cathode, we proposed a general scheme for the production of different hydrocarbon fuels as CO_2 reduction product selectively by tuning external bias potential. The results presented in this work clearly demonstrate that by proper selection and devising functional multi-layered hybrid composite cathode, it is possible to generate different hydrocarbon fuels selectively in PEC CO_2 reduction process just by controlling the bias potential. However, energy loss due to water splitting remains a challenge for improving the current efficiency of PEC CO_2 reduction under aqueous electrolytes, which needs further attention for commercial implementation of the process.

CRediT authorship contribution statement

The manuscript was prepared by **A.U. Pawar**, **U. Pal**, and **Y. S. Kang**. Concept of the work was formulated, designed, and executed by

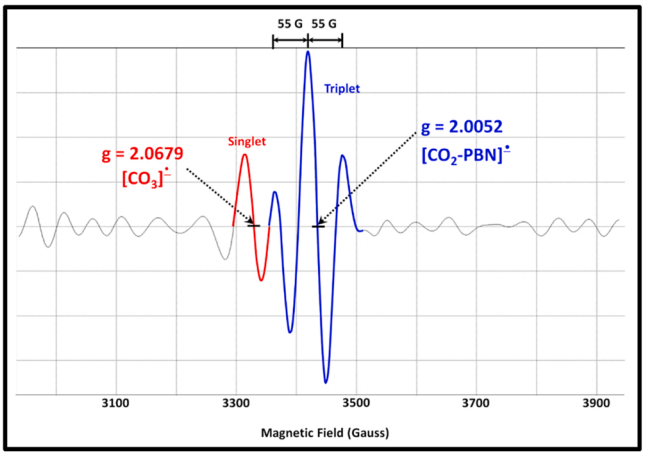

Fig. 7. Detecting the origin of $CO_2^{-\bullet}$ anion radicals by EPR spectroscopy. Simulated fitting EPR spectrum of $[CO_2{-}PBN]^{-\bullet}$ intermediate radicals (g = 2.0052, A = 55 G) formed during CO_2 reduction reaction over Cu/rGO/PVP/Nafion hybrid cathode. The minor signal with g = 2.0679 corresponds to $CO_3^{-\bullet}$ anion radicals formed due to reaction of CO_2 with the electrolyte (NaOH).

A. U. Pawar under the supervision of **Y. S. Kang**. The designs of CO_2 reduction and GC measurement systems were made by **C. W. Kim.**, **J. Y. Zheng** provided valuable inputs for the executed electrochemical studies. All the authors participated in the interpretation and discussion of results.

Declaration of Competing Interest

The authors declare that they have no known competing financial interests or personal relationships that could have appeared to influence the work reported in this paper.

Acknowledgements

This work financially supported by the Leader Project at the Sogang University funded by the Ministry of Science and ICT through the National Research Foundation of Korea (No. 2020R1A3B3079715). The authors extend their sincere thanks to Dr. Sun Hee Kim of the Western Seoul Center of Korea Basic Science Institute (KBSI) for providing EPR measurement facilities and to Dr. Weon-Sik Chae of Daegu Center of KBSI for their expertise and helps extended for TRPL measurements.

Appendix A. Supporting information

Supplementary data associated with this article can be found in the online version at doi:10.1016/j.apcatb.2021.120921.

References

[1] R. Priddle, et al. International EnergyAgency in World Energy Outlook 2011. ⟨http://www.worldenergyoutlook.org⟩.
[2] E.J. Maginn, What to do with CO_2, J. Phys. Chem. Lett. 1 (2010) 3478–3479, https://doi.org/10.1021/jz101582c.
[3] M. Aresta, A. Dibenedetto, Utilization of CO_2 as a chemical feedstock: opportunities and challenges, Dalton Trans. 27 (2007) 2975–2992, https://doi.org/10.1039/B700658F.
[4] J.P. Smol, How is life on earth reacting to climate change? Nature 483 (2012) S12–S15. ⟨https://www.nature.com/articles/483S12a⟩.
[5] M. Mikkelsen, M. Jorgensen, F.C. Krebs, The teraton challenge a review of fixation and transformation of carbon dioxide, Energy Environ. Sci. 3 (2010) 43–81, https://doi.org/10.1039/B912904A.
[6] A. Bansode, A. Urakawa, Towards full one-pass conversion of carbon dioxide to methanol and methanol-derived products, J. Catal. 309 (2014) 66–70, https://doi.org/10.1016/j.jcat.2013.09.005.
[7] H.R. Park, A.U. Pawar, U. Pal, T. Zhang, Y.S. Kang, Enhanced solar photoreduction of CO_2 to liquid fuel over rGO grafted NiO-CeO_2 heterostructure nanocomposite,

Nano Energy 79 (105483) (2021) 1–10, https://doi.org/10.1016/j.nanoen.2020.105483.
[8] X. Zhao, Y. Xia, H. Li, X. Wang, X. Jiao, D. Chen, Oxygen vacancy dependent photocatalytic CO_2 reduction activity in liquid-exfoliated atomically thin BiOCl nanosheets, Appl. Catal. B Environ. 297 (2021), 120426, https://doi.org/10.1016/j.apcatb.2021.120426.
[9] Y. Zhang, Z. Xu, Q. Wang, W. Hao, X. Zhai, X. Fei, X. Huang, Y. Bi, Unveiling the activity origin of ultrathin BiOCl nanosheets for photocatalytic CO_2 reduction, Appl. Catal. B Environ. (2021), https://doi.org/10.1016/j.apcatb.2021.120679.
[10] X. Hu, Z. Xie, Q. Tang, H. Wang, L. Zhang, J. Wang, Enhanced CH_4 yields by interfacial heating-induced hot water steam during photocatalytic CO_2 reduction, Appl. Catal. B Environ. 298 (2021), 120635, https://doi.org/10.1016/j.apcatb.2021.120635.
[11] Y. Wang, Q. Zhou, Y. Zhu, D. Xu, High efficiency reduction of CO_2 to CO and CH4 via photothermal synergistic catalysis of lead-free perovskite $Cs_3Sb_2I_9$, Appl. Catal. B Environ. 294 (2021), 120236, https://doi.org/10.1016/j.apcatb.2021.120236.
[12] C. Xu, X. Zhang, M.N. Zhu, L. Zhang, P.F. Sui, R. Feng, Y. Zhang, J.L. Luo, Accelerating photoelectric CO_2 conversion with a photothermal wavelength-dependent plasmonic local field, Appl. Catal. B Environ. 298 (2021), 120533, https://doi.org/10.1016/j.apcatb.2021.120533.
[13] A.A. Peterson, et al., How copper catalyzes the electroreduction of carbon dioxide into hydrocarbon fuels, Energy Environ. Sci. 3 (2010) 1311–1315, https://doi.org/10.1039/C0EE00071J.
[14] J.Y. Kim, C.H. Ryu, J.H. Lee, A.U. Pawar, W.D. Jang, Y.S. Kang, H.S. Ahn, Electrodeposited CuAgHg multimetallic thin films for improved CO_2 conversion: dramatic impact of hg incorporation on product selectivity, ACS Appl. Energy Mater 7 (3) (2020) 6670–6677, https://doi.org/10.1021/acsaem.0c00784.
[15] W. Choi, M. Kim, B. Kim, Y. Park, D.S. Han, M.R. Hoffmann, H. Park, Electrocatalytic arsenite oxidation in bicarbonate solutions combined with CO_2 reduction to formate, Appl. Catal. B Environ. 265 (2020), 118607, https://doi.org/10.1016/j.apcatb.2020.118607.
[16] M.T. Tang, H. Peng, P.S. Lamoureus, M. Bajdich, F.A. Pedersen, From electricity to fuels: descriptors for C1 selectivity in electrochemical CO_2 reduction, Appl. Catal. B Environ. 279 (2020), 119384, https://doi.org/10.1016/j.apcatb.2020.119384.
[17] L. Wang, P. Liu, Y. Xu, Y. Zhao, N. Xue, X. Guo, L. Peng, Y. Zhu, M. Ding, Q. Wang, W. Ding, Enhanced catalytic activity and stability of bismuth nanosheets decorated by 3-aminopropyltriethoxysilane for efficient electrochemical reduction of CO_2, Appl. Catal. B Environ. 298 (2021), 120602, https://doi.org/10.1016/j.apcatb.2021.120602.
[18] J. Shi, et al., Enzymatic conversion of carbon dioxide, Chem. Soc. Rev. 44 (2015) 5981–6000, https://doi.org/10.1039/C5CS00182J.
[19] C.W. Kim, M.J. Kang, S. Ji, Y.S. Kang, Artificial photosynthesis for formaldehyde production with 85% of Faradaic efficiency by tuning the reduction potential, ACS Catal. 8 (2) (2018) 968–974, https://doi.org/10.1021/acscatal.7b02953.
[20] M.J. Kang, C.W. Kim, H.G. Cha, A.U. Pawar, Y.S. Kang, Selective liquid chemicals on CO_2 reduction by energy level tuned rGO/TiO_2 dark cathode with $BiVO_4$ photoanode, Appl. Catal. B Environ. 295 (1–10) (2021), 120267, https://doi.org/10.1016/j.apcatb.2021.120267.
[21] Y. Zhang, Q. Li, C. Liu, X. Shan, X. Chen, W. Dai, X. Fu, The promoted effect of a metal-organic frameworks (ZIF-8) on Au/TiO_2 for CO oxidation at room temperature both in dark and under visible light irradiation, Appl. Catal. B Environ. 224 (2018) 283–294, https://doi.org/10.1016/j.apcatb.2017.10.027.
[22] J.C. Cardoso, S. Stulp, J.F. de Brito, J.B.S. Flor, R.C.G. Frem, M.V.B. Zanoni, MOFs based on ZIF-8 deposited on TiO2 nanotubes increase the surface adsorption of CO_2 and its photoelectrocatalytic reduction to alcohols in aqueous media, Appl. Catal. B Environ. 225 (2018) 563–573, https://doi.org/10.1016/j.apcatb.2017.12.013.
[23] Y. Dou, A. Zhou, Y. Yao, S.Y. Lim, J.R. Li, W. Zhang, Suppressing hydrogen evolution for high selective CO_2 reduction through surface-reconstructed heterojunction photocatalyst, Appl. Catal. B Environ. 286 (2021), 119876, https://doi.org/10.1016/j.apcatb.2021.119876.
[24] R.E. Blankenship, et al., Comparing photosynthetic and photovoltaic efficiencies and recognizing the potential for improvement, Science 332 (2011) 805–809, https://doi.org/10.1126/science.1200165.
[25] X.G. Zhu, S.P. Long, D.R. Ort, Improving photosynthetic efficiency for greater yield, Annu. Rev. Plant Biol. 61 (29) (2010) 1–29, 27, ⟨https://www.annualreviews.org/doi/10.1146/annurev-arplant-042809-112206⟩.
[26] F.C. Vallejo, M.T.M. Koper, Theoretical considerations on the electroreduction of CO to C_2 species on Cu (100) electrodes, Angew. Chem. Int. Ed. 52 (2013) 7282–7285, https://doi.org/10.1002/anie.201301470.
[27] X. Nie, M.R. Esopi, M.J. Janik, A. Asthagiri, Selectivity of CO_2 reduction on copper electrodes: the role of the kinetics of elementary steps, Angew. Chem. Int. Ed. 52 (2013) 2459–2462, https://doi.org/10.1002/anie.201208320.
[28] J.H. Montoya, A.A. Peterson, J.K. Norskov, Insights into C-C coupling in CO_2 electroreduction on copper electrodes, Chem. Cat. Chem. 5 (2013) 737–742, https://doi.org/10.1002/cctc.201200564.
[29] K.J.P. Schouten, et al., A new mechanism for the selectivity to C_1 and C_2 species in the electrochemical reduction of carbon dioxide on copper electrodes, Chem. Sci. 2 (2011) 1902, https://doi.org/10.1039/C1SC00277E.
[30] T. Hatsukade, et al., Insights into the electrocatalytic reduction of CO_2 on metallic silver surfaces, Phys. Chem. Chem. Phys. 16 (2014) 13814–13819, https://doi.org/10.1039/C4CP00692E.
[31] R. Kortlever, et al., Catalysts and reaction pathways for the electrochemical reduction of carbon dioxide, J. Phys. Chem. Lett. 6 (2015) 4073–4082, https://doi.org/10.1021/acs.jpclett.5b01559.
[32] A.U. Pawar, C.W. Kim, M.T. Nguyen-Le, Y.S. Kang, General review on the components and parameters of photoelectrochemical system for CO_2 Reduction with in situ analysis, ACS Sustain. Chem. Eng. 7 (2019) 7431–7455, https://doi.org/10.1021/acssuschemeng.8b06303.
[33] D.T. Whipple, J.A. Kenis, Prospects of CO_2 utilization via direct heterogeneous electrochemical reduction, J. Phys. Chem. Lett. 1 (2010) 3451–3458, https://doi.org/10.1021/jz1012627.
[34] M. Gattrell, N. Gupta, A. Co, Electrochemical reduction of CO_2 to hydrocarbons to store renewable electrical energy and upgrade biogas, Energy Convers. Manag. 48 (2007) 1255–1265, https://doi.org/10.1016/j.enconman.2006.09.019.
[35] L. Zhang, D. Zhu, G.M. Nathanson, R.J. Hamers, Selective photoelectrochemical reduction of aqueous CO_2 to CO by solvated electrons, Angew. Chem. Int. Ed. 53 (2014) 9746–9750, https://doi.org/10.1002/anie.201404328.
[36] E.E. Barton, D.M. Rampulla, A.B. Bocarsly, Selective solar-driven reduction of CO_2 to methanol using a catalyzed p-GaP Based photoelectrochemical cell, J. Am. Chem. Soc. 130 (2008) 6342–6344, https://doi.org/10.1021/ja0776327.
[37] M.J. Kang, C.W. Kim, A.U. Pawar, H.G. Cha, S. Ji, W.B. Cai, Y.S. Kang, Selective alcohol on dark cathodes by photoelectrochemical CO_2 valorization and their in situ characterization, ACS Energy Lett. 4 (7) (2019) 1549–1555, https://doi.org/10.1021/acsenergylett.9b00927.
[38] M. Zafrir, M. Ulman, Y. Zuckerman, M. Halmann, Photoelectrochemical reduction of carbon dioxide to formic acid, formaldehyde and methanol on p-Gallium arsenide in an aqueous V(II)-V(III) chloride redox system, J. Electroanal. Chem. Interfacial Electrochem. 159 (2) (1983) 373–389, https://doi.org/10.1016/S0022-0728(83)80635-4.
[39] A.A. Aguirre, J. Ojeda, J.F. Brito, S.G. Segura, M.V.B. Zanoni, H. Alarcon, Photoelectrodes of Cu_2O with interfacial structure of topological insulator Bi_2Se_3 contributes to selective photoelectrocatalytic reduction of CO_2 towards methanol, J. CO2 Util. 39 (1–8) (2020), 101154, https://doi.org/10.1016/j.jcou.2020.101154.
[40] C. Hu, et al., Spontaneous reduction and assembly of graphene oxide into three-dimensional graphene network on arbitrary conductive substrates, Sci. Rep. 3 (1–10) (2013) 2065, https://doi.org/10.1038/srep02065.
[41] S. George, et al., Role of Fe doping in tuning the band gap of TiO_2 for the photo-oxidation-induced cytotoxicity paradigm, J. Am. Chem. Soc. 133 (2011) 11270–11278, https://doi.org/10.1021/ja202836s.
[42] J.G. Ma, et al., The electronic structures and optical properties of alkaline-earth metals doped anatase TiO_2: a comparative study of screened hybrid functional and generalized gradient approximation, Materials 8 (2015) 5508–5525, https://doi.org/10.3390/ma8085257.
[43] A.A. Peterson, et al., How copper catalyzes the electroreduction of carbon dioxide into hydrocarbon fuels, Energy Environ. Sci. 3 (2010) 1311–1315, https://doi.org/10.1039/C0EE00071J.
[44] Y. Hori, K. Kikuchi, A. Murata, S. Suzuki, Production of methane and ethylene in electrochemical reduction of carbon dioxide at copper electrode in aqueous hydrogencarbonate solution, Chem. Lett. (1986) 897–898, https://doi.org/10.1246/cl.1986.897.
[45] E.M. Kock, et al., In situ FT-IR spectroscopic study of CO_2 and CO adsorption on Y_2O_3, ZrO_2, and yttria-stabilized ZrO_2, J. Phys. Chem. C 117 (2013) 17666–17673, https://doi.org/10.1021/jp405625x.
[46] A. Masala, et al., New insights into UTSA-16, Phys. Chem. Chem. Phys. 18 (2016) 220–227, https://doi.org/10.1039/c5cp05905d.
[47] I.V. Chernyshova, P. Somasundaran, S. Ponnurangam, On the origin of the elusive first intermediate of CO_2 electroreduction, Proc. Natl. Acad. Sci. USA 115 (40) (2018) E9261–E9270, https://doi.org/10.1073/pnas.1802256115.
[48] P.T. Andrew, A.C. Joe, J.D. Trevor, Surface-enhanced resonance Raman spectroscopy of Ru and Os polyvinylpyridine adsorbed on silver electrodes, J. Chem. Soc., Faraday Trans. 93 (9) (1997) 1803–1812, https://doi.org/10.1039/A608368D.
[49] Z. Idris, K.J. Jens, D.A. Eimer, Speciation of MEA-CO_2 adducts at equilibrium using Raman spectroscopy, Energy Procedia 63 (2014) 1424–1431, https://doi.org/10.1016/j.egypro.2014.11.152.
[50] T. Reda, C.M. Plugge, N.J. Abram, J. Hirst, Reversible interconversion of carbon dioxide and formate by an electroactive enzyme, Proc. Natl. Acad. Sci. USA 105 (31) (2008) 10654–10658, https://doi.org/10.1073/pnas.0801290105.
[51] E.G. Janzen, R.A. Towner, M. Brauer, Factors influencing the formation of the carbon dioxide anion ($\bullet CO_2^-$) spin adduct of PBN in the rat liver metabolism of halocarbons, Free Radic. Res. Commun. 4 (6) (1987) 359–369, https://doi.org/10.3109/10715768809066904.
[52] D.M.F. Santos, C.A.C. Sequeira, J.L. Figueiredo, Hydrogen production by alkaline water electrolysis, Quim. Nova 36 (8) (2013) 1176–1193, https://doi.org/10.1590/S0100-40422013000800017.